Chiral phase structure of three flavor QCD at vanishing baryon number density

A. Bazavov, H.-T. Ding, P. Hegde, F. Karsch, E. Laermann, Swagato Mukherjee, P. Petreczky, and C. Schmidt

Phys. Rev. D **95**, 074505 — Published 12 April 2017

DOI: 10.1103/PhysRevD.95.074505

Chiral phase structure of three flavor QCD at vanishing baryon number density

A. Bazavov[a], H.-T. Ding[b], P. Hegde[c], F. Karsch[d,e], E. Laermann[d],
Swagato Mukherjee[e], P. Petreczky[e] and C. Schmidt[d]

[a]*Department of Computational Mathematics, Science and Engineering,*
Department of Physics and Astronomy, Michigan State University, East Lansing, Michigan, 48824, USA
[b]*Key Laboratory of Quark & Lepton Physics (MOE) and Institute of Particle Physics,*
Central China Normal University, Wuhan 430079, China
[c]*Center for High Energy Physics, Indian Institute of Science, Bangalore 560012, India*
[d]*Fakultät für Physik, Universität Bielefeld, D-33615 Bielefeld, Germany*
[e]*Physics Department, Brookhaven National Laboratory, Upton, NY 11973, USA*

We investigate the phase structure of QCD with 3 degenerate quark flavors as function of the degenerate quark masses at vanishing baryon number density. We use the Highly Improved Staggered Quarks on lattices with temporal extent $N_t = 6$ and perform calculations for six values of quark masses, which in the continuum limit correspond to pion masses in the range 80 MeV $\lesssim m_\pi \lesssim$ 230 MeV. By analyzing the volume and temperature dependence of the chiral condensate and chiral susceptibility we find no direct evidence for a first order phase transition in this range of pion mass values. Relying on the universal scaling behaviors of the chiral observables near an anticipated chiral critical point, we estimate an upper bound for the critical pion mass, $m_\pi^c \lesssim 50$ MeV, below which a region of first order chiral phase transition is favored.

PACS numbers: 11.15.Ha, 12.38.Gc, 25.75.Nq

I. INTRODUCTION

Mapping out the QCD phase diagram is one of the basic goals of lattice QCD calculations at non-zero temperature. It was noted by Pisarski and Wilczek that the order of the chiral phase transition in QCD may depend on the number of light quark degrees of freedom and qualitative features of the transition may also change with the quark mass [1]. In QCD with 3 massless quark flavors the chiral phase transition is expected to be first order. If this is the case, the phase transition remains first order even for non-zero values of the quark masses and terminates at a critical quark mass m_q^c, or equivalently at a critical pion mass, m_π^c, where the transition becomes second order belonging to the 3-d Z(2) Ising universality class. For quark mass $m_q > m_q^c$ chiral restoration takes place through a smooth crossover.

Knowledge about the phase structure in the light-strange quark mass plane at vanishing chemical potential also impacts our understanding regarding its extension to non-zero chemical potential. For zero chemical potential, the values of critical quark masses characterize a line of chiral phase transitions in the light-strange quark mass plane. This line extends toward the non-zero chemical potential direction and forms a surface of phase transitions in the 3-d, Z(2) universality class. The chemical potential where this surface intersects the physical values of light and strange quark masses may correspond to the QCD critical point [2]. However, determining the curvature of this surface turns out to be complicated [3, 4] and, in fact, is likely to suffer from similar lattice cut-off effects as those contributing to the value of the critical pion mass itself[1].

The first order chiral phase transition in 3–flavor QCD has been investigated on coarse lattices using unimproved [6–9] as well as improved actions [2, 10–15]. However, on these coarse lattices the critical pion mass value turns out to be strongly cut-off and regularization scheme dependent. As of now no continuum extrapolated results exist. Current results for the critical pion mass obtained in calculations with staggered (standard and p4fat3) fermions on $N_\tau = 4$ and 6 lattices vary from about 300 MeV down to about 70 MeV [2, 6–13]. While studies using the clover improved Wilson fermion action on $N_t = 4$, 6, 8 and 10 lattices suggest that m_π^c can change from about 750 MeV to about 100 MeV [14, 15]. In general it is found that the critical pion mass decreases when using either improved actions or when reducing the lattice spacing[2].

In addition to studies concerning N_f=3, lattice QCD calculations searching for first order chiral phase transitions in other cases have also been carried out. Studies on N_f=2 QCD using standard staggered fermions [17] and unimproved Wilson fermions [18] on $N_t = 4$ lattices suggest that m_π^c is nonzero and could be around 560 MeV. Investigations on $N_t = 6$ lattices have also been performed using an improved staggered fermion action (2stout action), in which the

[1] Other possibilities for generating a second order transition at the physical values of quark masses have been discussed in Ref. [5].
[2] A study of 4-flavor QCD using HYP action [16] also suggests that the first order chiral phase transition becomes weaker in the continuum limit.

three quark flavors are not taken to be degenerate. Instead the ratio of light to strange quark masses has been kept fixed to about 1/27 when approaching the massless limit [19]. The analysis of Ref. [19] suggests that m_π^c is around 50 MeV. While a recent study on QCD with two degenerate light quarks approaching to chiral limit and a fixed physical strange quark mass using the Highly Improved Staggered Quark (HISQ) action on $N_\tau = 6$ lattices suggests that m_π^c is compatible with zero [20].

To advance the understanding of the chiral phase transition in 3-flavor QCD we study the chiral phase structure at vanishing baryon density using the HISQ action on lattices with temporal extent $N_\tau = 6$. Preliminary results have been reported in conference proceedings [20–22]. The paper is organized as follows. In section II we give details on the parameters used in our calculations. In section III we describe the universal properties in the vicinity of the chiral phase transition and chiral observables. In section IV we present our results on the phase structure of 3-flavor QCD and finally we summarize in section V.

II. LATTICE FORMULATION AND SETUP

It has been noted previously that the estimate of the critical pion mass m_π^c from lattice QCD calculations strongly depends on lattice cutoff effects. In order to reach a better understanding of the first order chiral phase transition region we use here the HISQ action [23]. At a given value of the lattice spacing the HISQ action achieves better taste symmetry than the asqtad, p4 and 2stout actions, which previously have been used for the analysis of the phase structure of 3-flavor QCD [24]. Furthermore, we use a tree-level improved Symanzik gauge action and perform calculations on lattices with temporal extent N_t=6. The calculations have been performed for 3 degenerate quark flavors at six different values of quark masses m_q (in units of the lattice spacing) in the range $0.0009375 \leq m_q \leq 0.0075$. Gauge configurations have been generated with a rational hybrid Monte Carlo (RHMC) algorithm. The chiral observables (introduced below) were measured after every 10th trajectory of unit length using 40 Gaussian-distributed stochastic sources.

To convert our simulation parameters to physical units we use results on the determination of the lattice spacings in (2+1)-flavor QCD obtained by the HotQCD collaboration [25, 26]. The lattice spacing is fixed using the r_0 scale [25] and hadron masses calculated on lines of constant physics. To be specific, for a fixed ratio of the light to strange quark masses, $m_l/m_s = 1/20$, the hadron masses have been determined by demanding that the strange quark mass attains its physical value. In order to use this for our 3-flavor analysis we take into account that the lattice spacing at a given value of the gauge coupling depends on the quark masses, i.e. as we vary the quark masses the value of r_0 in lattice units, r_0/a, will change. Using results for r_0/a obtained in calculations for (2+1)-flavor QCD with two different values of the light to strange quark mass ratio, $m_l = m_s/5$ [25] and $m_l = m_s/20$ [25, 26], we can estimate the dependence of r_0/a at fixed values of the gauge coupling $\beta = 10/g^2$, on the quark mass combination $m_s + 2m_l$. Assuming that r_0/a only depends on this combination of the quark masses we can estimate its value for the case of three degenerate flavors for different values of the quark mass, m_q. We find that for the lightest quark mass $m_q = m_s/80 = 0.0009375$ the change in r_0/a in the relevant range of gauge couplings $5.8 \leq \beta \leq 6.1$ amounts to $\sim 4\%$. For example, for $N_f = 3$ with $m_q = 0.0009375$ and close to the critical coupling $\beta = 5.85$ the estimated value is $r_0/a = 1.82$. In comparison, the corresponding value for $N_f = 2 + 1$ with physical m_s and $m_l = m_s/20$ is $r_0/a = 1.75$.

Since the dependence of the lattice scale on quark masses seems to be moderate down to the smallest quark mass value used in our study, we estimate the value of pseudo-scalar meson masses relevant for our choice of parameters by simply rescaling the pion mass obtained in the (2+1)-flavor studies by the corresponding ratio of the light quark masses, i.e. by $\sqrt{m_q/m_l}$. From this we find that the range of quark mass values explored by us corresponds to masses for the lightest pseudo-scalar meson in the range 80 MeV $\lesssim m_\pi \lesssim$ 230 MeV. In the continuum limit this corresponds to the value of the pion mass. For the spatial size of the lattice we generally use $N_s = 24$. This ensures that the product of pion mass and spatial extent $L = N_s a$ stays large also for the lightest quark masses, i.e. $m_\pi L \gtrsim 3$. At the second largest and smallest value of the quark masses used by us, $m_q = 0.00375$ and $m_q = 0.0009375$, respectively, we also performed simulations for different spatial lattice sizes. We used four different lattice sizes for the second heaviest quark mass, $N_s = 10$, 12, 16 and 24, and two lattice sizes for the lightest quark mass, $N_s = 16$ and 24. The simulation parameters and corresponding pion masses in the continuum limit are listed in Table I.

The basic observables used in our analysis are the chiral condensate

$$\frac{\langle\bar{\psi}\psi\rangle_{\rm q}}{T^3} \;=\; \frac{1}{3}\frac{1}{VT^2}\frac{\partial \ln Z}{\partial m_q} = \frac{N_t^2}{4N_s^3}\left\langle {\rm Tr}\, D^{-1}(m_q)\right\rangle , \tag{1}$$

and the disconnected part of the chiral susceptibility

$$\frac{\chi_{\rm q,disc}}{T^2} \;\equiv\; \frac{N_t}{16N_s^3}\left(\left\langle \left({\rm Tr}\, D^{-1}(m_q)\right)^2\right\rangle - \left\langle {\rm Tr}\, D^{-1}(m_q)\right\rangle^2\right) , \tag{2}$$

$N_s^3 \times N_t$	m_q	m_π [MeV]	# β values	average # of conf. for each β
$16^3 \times 6$	0.0075	230	9	1000
$24^3 \times 6$	0.00375	160	11	2000
$16^3 \times 6$	0.00375	160	8	2000
$12^3 \times 6$	0.00375	160	9	2000
$10^3 \times 6$	0.00375	160	11	1500
$24^3 \times 6$	0.0025	130	7	1300
$24^3 \times 6$	0.001875	110	8	1000
$24^3 \times 6$	0.00125	90	7	1000
$24^3 \times 6$	0.0009375	80	8	1500
$16^3 \times 6$	0.0009375	80	8	1500

TABLE I: Parameters used in simulations of 3-flavor QCD using the HISQ action and the tree-level improved Symanzik gauge action.

where Z denotes the QCD partition function and D is the staggered fermion matrix. The chiral condensate and the chiral susceptibility are normalized to one flavor degree of freedom.

III. UNIVERSAL PROPERTIES NEAR A CRITICAL POINT

In the vicinity of a critical point the free energy of a system can be expressed as a sum of a singular and a regular part,

$$f = -\frac{T}{V}\ln Z \equiv f_{\rm sing}(T, m_q) + f_{\rm reg}(T, m_q). \tag{3}$$

The singular contribution is given in terms of a scaling function and critical exponents characteristic for the universality class of the critical point,

$$f_{\rm sing}(T, m_q) = h_0 h^{1+1/\delta} f_s(z)\ ,\ z = t/h^{1/\beta\delta}\ . \tag{4}$$

Here β and δ are universal critical exponents, h_0 is a non-universal normalization factor, t and h are reduced temperature and symmetry breaking parameters, respectively. They vanish at the critical point, $(t, h) = (0, 0)$, and are functions of the couplings, T and m. For the 3-dimensional Z(2) universality class the critical exponents $\beta = 0.3207$, $\delta = 4.7898$ and $\gamma = \beta(\delta - 1) = 1.2371$ [27].

The singular part of the free energy density, $f_{\rm sing}(T, m)$, dominates over the regular part when the system is close to the critical region. The order parameter M of the transition and its susceptibility χ_M are then governed by scaling functions that arise from the scaling form of the singular part of the free energy [28, 29]

$$\begin{aligned} M(t,h) &= -\partial f_{\rm sing}(t,h)/\partial H = h^{1/\delta}\, f_G(z), &(5)\\ \chi_M &= \frac{\partial M}{\partial H} = \frac{1}{h_0} h^{1/\delta-1} f_\chi(z), &(6)\end{aligned}$$

where $f_G(z) = -\left(1+\frac{1}{\delta}\right) f_s(z) + \frac{z}{\beta\delta}\frac{\partial f_s(z)}{\partial z}$ and $f_\chi(z) = \frac{1}{\delta}\left(f_G(z) - \frac{z}{\beta}\frac{\partial f_G(z)}{\partial z}\right)$ are universal scaling functions. The variables t and h are related to the temperature T and the symmetry breaking (magnetic) field $H \equiv h_0 h$. The order parameter susceptibility may be used to introduce a variable t_p as the pseudo-critical temperature, which is defined as the location of the maximum of χ_M obtained as a function of t for fixed h. This is reached for some value $z_p = t_p/h^{1/\beta\delta}$. One thus finds the standard scaling behavior of χ_M^{peak} as a function of the external field h

$$\chi_M^{peak} \sim h^{1/\delta-1} f_\chi(z_p)\ . \tag{7}$$

The generic discussion of the scaling behavior of the order parameter and its susceptibility given above becomes more complicated in cases where the scaling variables t and h cannot directly be mapped onto corresponding couplings of the theory under study, e.g. 3-flavor QCD. If 3-flavor QCD has a first order transition in the chiral limit, a second order transition at non-vanishing values of the quark mass exists, which terminates the line of first order transitions. This critical endpoint is expected to be in the $Z(2)$ universality class [30]. The relevant fields in the vicinity of this critical point can be expressed as linear combinations of $m_q - m_q^c$ and $T - T_c$ [31]. Here T_c is the transition temperature at vanishing external field h, which in 3-flavor QCD calculations is related to a critical coupling β_c and a critical quark mass m_q^c. Rather than using the temperature $T - T_c$ it is convenient for our discussion to use the difference of gauge couplings $\beta = 10/g^2$ (not to be confused with the critical exponent β)[3]. The variables t and h may then be related to the bare couplings of 3-flavor QCD,

$$
\begin{aligned}
t &= (\beta - \beta_c + A\ (m_q - m_q^c))/t_0 \ , &(8)\\
h &= (m_q - m_q^c + B\ (\beta - \beta_c))/h_0 \ . &(9)
\end{aligned}
$$

Although it is not necessarily the case one may assume that the temperature-like (t) and external-field-like (h) direction are orthogonal to each other. In that case $B = -A$.

Let us first discuss the scaling behavior of the order parameter susceptibility in terms of the bare QCD parameters $\Delta m \equiv m_q - m_q^c$ and $\Delta\beta \equiv \beta - \beta_c$. In the $(\Delta\beta)$-(Δm) coordinate frame the constant value of the scaling variable z is given by

$$
z_p = z_0 \, \frac{\Delta\beta - B\Delta m}{(\Delta m + B\Delta\beta)^{1/\beta\delta}} \ . \tag{10}
$$

Here $z_0 = h_0^{1/\beta\delta}/t_0$. The above equation fixes the relation between $\Delta\beta$ and Δm required to keep z_p constant. Obviously for $B = 0$ one just recovers the scaling relation $\Delta m = (\Delta\beta\, z_0/z_p)^{\beta\delta}$. For $B \neq 0$ we obtain for $\Delta\beta \to 0$,

$$
\Delta m = -B\Delta\beta + \left(\frac{z_0}{z_p}(1+B^2)\Delta\beta\right)^{\beta\delta} + \mathcal{O}((\Delta\beta)^{2\beta\delta-1}) \ . \tag{11}
$$

As $\beta\delta > 1$ for the universality classes of interest to us the first term in this relation will always dominate in the limit $\Delta\beta \to 0$ and one finds from Eqs. (7)-(9),

$$
\chi_M^{peak} \sim h^{1/\delta - 1} \sim \begin{cases} (\Delta m)^{-(1-1/\delta)} & , \ B = 0, \\ (\Delta m)^{-\gamma} & , \ B \neq 0 \ . \end{cases} \tag{12}
$$

For any $B \neq 0$ the susceptibility of the order parameter thus will diverge with the critical exponent γ rather than $1 - 1/\delta < \gamma$ when approaching the critical point at fixed $z = z_p$. Similarly one finds for the order parameter at the critical gauge coupling β_c,

$$
M_c \sim h^{1/\delta} \sim \begin{cases} (\Delta m)^{1/\delta} & , \ B = 0, \\ (\Delta m)^{\beta} & , \ B \neq 0 \ . \end{cases} \tag{13}
$$

In an actual lattice QCD calculation we do not directly deal with the order parameter M and its susceptibility χ_M. The proper order parameter M, which detects the breaking of the $Z(2)$ symmetry and vanishes in the symmetry restored phase, can be constructed from two independent thermodynamic observables, e.g. a linear combination of the chiral condensate $\langle\bar\psi\psi\rangle$ and the pure gauge action S_G (or second order quark number susceptibility χ_2^q) [10]. Similarly the susceptibility of the order parameter receives contributions from several terms, among these is the disconnected part of the chiral susceptibility. Thus it may be expected that the singular behavior of chiral condensates $\langle\bar\psi\psi\rangle$ and its disconnected chiral susceptibilities χ_q obey the relations given in Eqs. (13) and (12), respectively. In Appendix A we give some more details on this and the corrections to scaling that arise from the fact that the chiral condensate and its susceptibility are not the correct order parameter and order parameter susceptibility for the Z(2) symmetry breaking in 3-flavor QCD.

---

[3] In the continuum limit the gauge coupling β and the temperature $T = 1/(aN_t)$ are related through the asymptotic scaling relation, $T/\Lambda = \exp(\beta/(20b_0))$, with b_0 denoting the coefficient of the leading term in the QCD β-function. For small temperature differences, i.e. in the vicinity of a critical point one thus finds $(T - T_c)/T_c = \beta - \beta_c$.

IV. RESULTS

A. Chiral condensates and chiral susceptibilities

In Fig. 1 (left) we show the chiral condensates as function of the gauge coupling β for various values of the quark masses corresponding to the pion masses ranging from 230 MeV down to 80 MeV. All data shown in this figure have been obtained on $24^3 \times 6$ lattices except those for the largest quark mass, $m_q = 0.0075$, corresponding to $m_\pi \simeq 230$ MeV, which are obtained on $16^3 \times 6$ lattices. Obviously, the chiral condensate decreases with increasing value of β, i.e. increasing temperature, as well as with decreasing quark mass. However, the slope of $\langle\bar\psi\psi\rangle$ seems to vary only little with β which differs from the behavior expected from an order parameter close to a critical temperature. This may reflect the fact that $\langle\bar\psi\psi\rangle$ is not the true order parameter for the transition we are trying to probe.

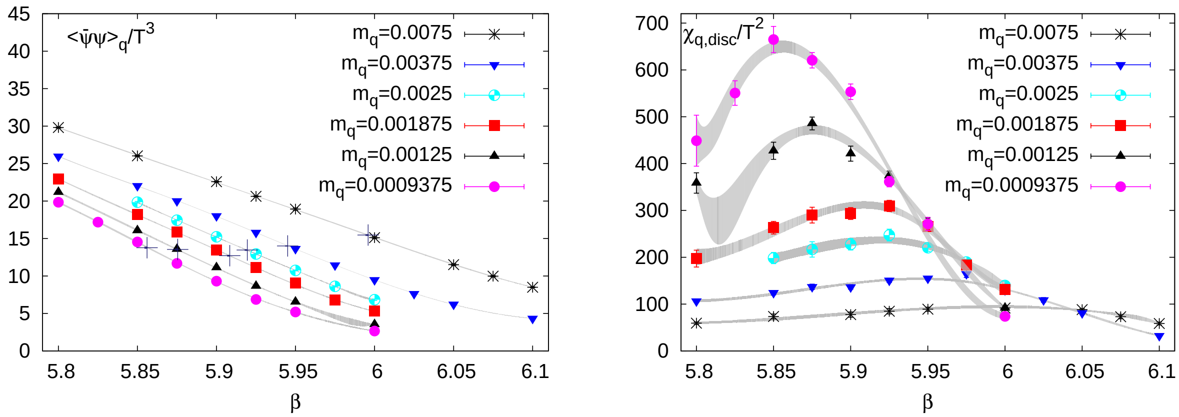

FIG. 1: The chiral condensates (left) and the disconnected part of the chiral susceptibilities (right) versus the gauge coupling β for various values of the bare quark masses m_q. Shaded curves show spline fits to the chiral observables (for more details see subsection IV C). Crosses shown in the left plot indicate values for the chiral condensate at the pseudo-critical values of the gauge coupling $\beta_c(m_q)$ determined from the location of the peaks of the disconnected chiral susceptibility. Here the results for $m_q < 0.0075$ are obtained on $24^3 \times 6$ lattices while those for $m_q = 0.0075$ are obtained on $16^3 \times 6$ lattices.

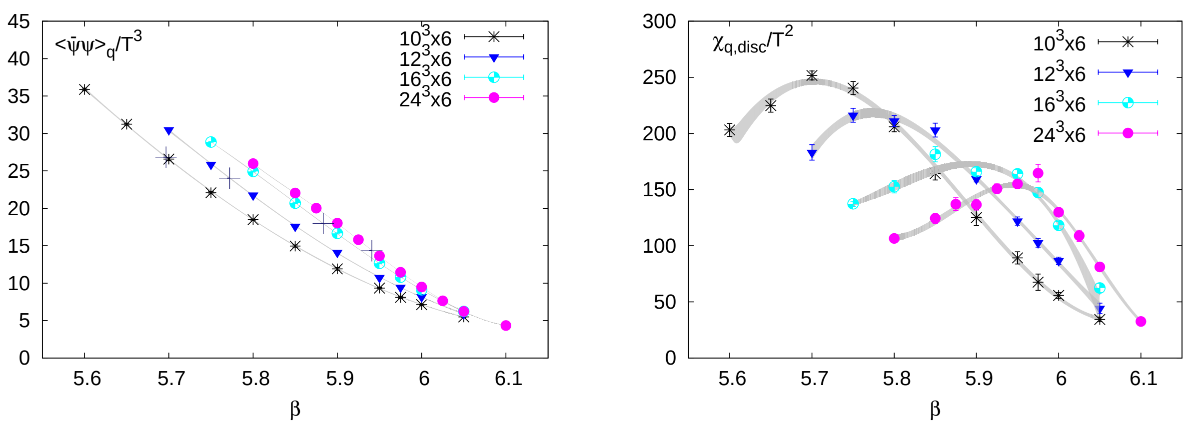

FIG. 2: Volume dependences of the chiral condensate (left) and the disconnected chiral susceptibility (right) with quark mass $m_q = 0.00375$ corresponding to $m_\pi \simeq 160$ MeV in the continuum limit. Bands in both plots denote interpolations via spline fits and the 'crosses' in the left plot label the critical gauge coupling extracted from the spline fits to disconnected susceptibilities.

In Fig. 1 (right) we show the temperature and quark mass dependence of the disconnected part of the chiral susceptibilities. They rise with decreasing values of the quark mass and has well defined peaks that shift to smaller values of the coupling β as the quark mass decreases, i.e. the pseudo-critical temperature of 3-flavor QCD decreases with decreasing values of the quark mass. The value of the chiral condensate at the pseudo-critical couplings, $\beta_c(m_q)$, is also indicated by crosses in Fig. 1 (left). The decrease of the transition temperature with decreasing value of the quark masses is well established in QCD thermodynamics and can qualitatively be understood in terms of the quark mass dependence of hadronic degrees of freedom. With decreasing quark mass they become lighter and are thus more easily excited in a thermal heat bath. They then contribute to the energy density of the system already at lower temperatures and can trigger the onset of a phase transition at a lower temperature.

The volume dependences of the chiral condensates and chiral susceptibilities at $m_q = 0.00375$ are shown in Fig. 2. Results obtained for four different volumes, i.e. N_s=10, 12, 16 and 24 are presented. As seen from Fig. 2 (left), at a fixed value of the temperature the chiral condensate increases as the volume is increased and this volume dependence is stronger at low temperature than at high temperature. The volume dependence of the disconnected part of the chiral susceptibilities is shown in Fig. 2 (right). The peak location of the disconnected susceptibilities, which defines the pseudo-critical temperature, shifts to higher temperatures and the peak height decreases when the volume increases.

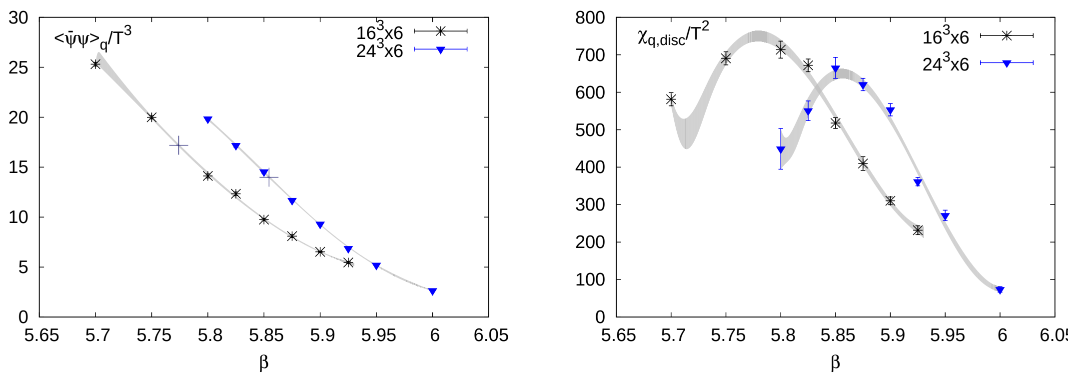

FIG. 3: Same as Fig. 2 but for $m_q = 0.0009375$ corresponding to $m_\pi \simeq 80$ MeV in the continuum limit.

Corresponding results for the volume dependence of $\langle\bar{\psi}\psi\rangle_q$ and $\chi_{q,disc}$ obtained for the lightest quark mass value, $m_q = 0.0009375$ ($m_\pi \approx 80$ MeV) are shown in Fig. 3. The pattern seen in the volume dependence of the chiral condensate and the chiral susceptibility is similar to the one shown for $m_q = 0.00375$ ($m_\pi \approx 160$ MeV) in Fig. 2. In particular, we note that also for this small quark mass value the peak height of the chiral susceptibility decreases with increasing volume.

This volume dependence is consistent with the expected volume dependence in the presence of a non-vanishing symmetry breaking field [32, 33]. In a finite volume chiral symmetry is not broken, i.e. the chiral condensate vanishes in the chiral limit at any value of the temperature. However, when taking first the infinite volume limit and then the chiral limit the chiral condensate can approach a non-zero value. One thus expects that for small values of the quark mass the condensate will increase as the volume increases and the volume dependence is larger at low temperatures than at high temperatures, because the asymptotic value of the chiral condensate is larger at low temperatures than at high temperatures. As the condensate will drop to zero in any finite volume, it also varies more rapidly with quark mass, which is reflected by the larger peak height of the chiral susceptibility in a finite volume.

B. Phase structure in the current quark mass window

As noted in the previous section we find in the entire range of quark masses analyzed by us that the peak height of the chiral susceptibility decreases with increasing volume. There is no hint for an increase of the peak height with volume, which is what one would expect to happen in the vicinity of a second or first order phase transition. This indicates that there is no first order phase transition in the system with values of the quark mass down to $m_q = 0.0009375$.

This is also supported by an analysis of the volume dependence of histograms for the chiral condensate. In Fig. 4 such histograms are shown for the chiral condensate at our lightest quark mass $m_q = 0.0009375$ calculated for two different volumes, i.e. $N_s = 16$ at $\beta = 5.8$ and $N_s = 24$ at $\beta = 5.85$, which are close to the corresponding pseudo-critical couplings for this value of the quark mass, $\beta_c(m_q) \simeq 5.78$ for $N_s = 16$ and $\beta_c(m_q) \simeq 5.86$ for $N_s = 24$. There is no evidence that a double peak structure, which would be indicative for the appearance of a first order phase transition, would develop in these distributions as the volume increases. Thus there is no evidence for two co-existing phases.

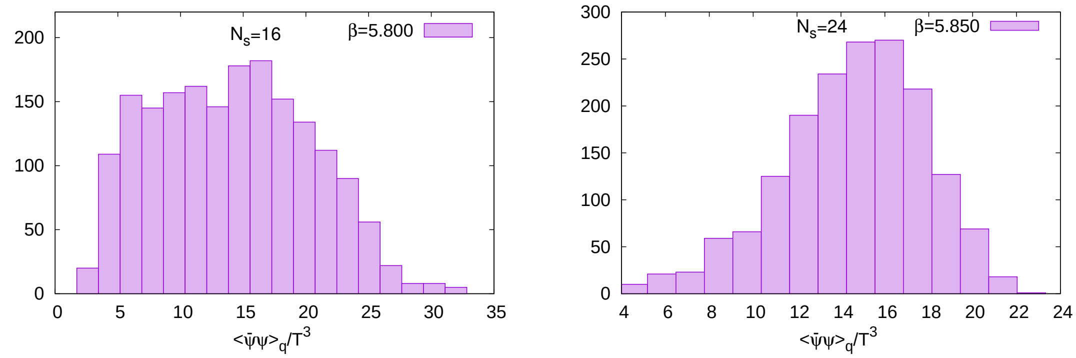

FIG. 4: The histogram of chiral condensates near β_c with $m_q = 0.0009375$ at $\beta = 5.800$ on $16^3 \times 6$ (left) and at $\beta = 5.850$ on $24^3 \times 6$ (right) lattices .

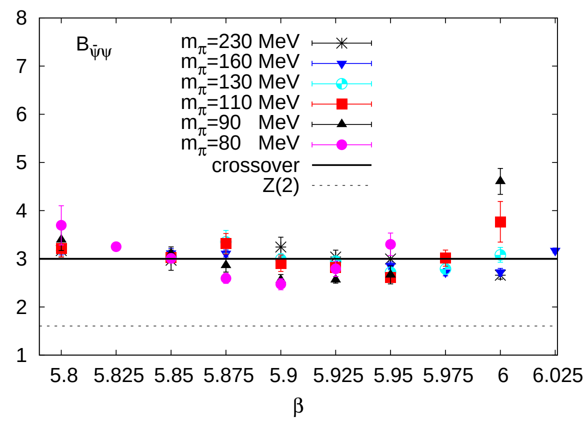

FIG. 5: The Binder cumulant of chiral condensates obtained from datasets with various values of pion masses.

We also analyzed the Binder cumulant $B_{\bar{\psi}\psi}$ of the chiral condensate at all values of the quark masses. $B_{\bar{\psi}\psi}$ is defined as follows

$$B_{\bar{\psi}\psi} = \frac{\langle(\delta\bar{\psi}\psi)^4\rangle}{\langle(\delta\bar{\psi}\psi)^2\rangle^2} , \tag{14}$$

where $\delta\bar{\psi}\psi = \bar{\psi}\psi - \langle\bar{\psi}\psi\rangle$ gives the deviation of the chiral condensate from its mean value on a given gauge field configuration. From different distributions of $\bar{\psi}\psi$ in different phases the value of $B_{\bar{\psi}\psi}$ can be obtained and can be used to distinguish phase transitions. For a first order phase transition, $B_{\bar{\psi}\psi} = 1$; for a crossover $B_{\bar{\psi}\psi} \simeq 3$; for a second order transition belonging to the 3-d Z(2) universality class, $B_{\bar{\psi}\psi} \simeq 1.6$. As seen from Fig. 5, the values of $B_{\bar{\psi}\psi}$ obtained from chiral condensates with different quark masses all lie around 3. There is a tendency for the lowest quark mass to give values smaller than 3 close to the crossover region. However, this clearly is not conclusive. Thus also the analysis of Binder cumulants presented in Fig. 5 suggests that 3-flavor QCD with pion masses ranging from 230 MeV to 80 MeV corresponds to systems with a smooth crossover transition.

In summary, all observables discussed above show no evidence for a first order phase transition in 3-flavor QCD with quark masses m_q ranging from 0.0075 down to 0.0009375.

C. Estimate of the critical pion mass

As discussed in the previous subsection we conclude that there is no first order phase transition even for quark masses as small as $m_q = 0.0009375$ ($m_\pi \approx 80$ MeV). However, we may test whether the chiral observables for different quark masses follow some specific scaling behaviors arising from the proximity of a chiral critical point. If such specific

lattice dim.	m_q	$\beta_c(m_q)$	$\chi^c_{\rm q,disc}/T^2$	$\langle\bar\psi\psi\rangle^c_q/T^3$
$16^3\times 6$	0.0075	6.00(3)	92(4)	15(2)
$24^3\times 6$	0.00375	5.941(8)	155(6)	14.3(7)
$16^3\times 6$	0.00375	5.88(2)	177(8)	18(2)
$12^3\times 6$	0.00375	5.77(2)	220(11)	24(2)
$10^3\times 6$	0.00375	5.70(2)	246(10)	27(1)
$24^3\times 6$	0.0025	5.92(2)	241(11)	14(2)
$24^3\times 6$	0.001875	5.90(1)	309(14)	13(1)
$24^3\times 6$	0.00125	5.87(1)	463(21)	14(1)
$24^3\times 6$	0.0009375	5.854(7)	649(28)	14.0(7)
$16^3\times 6$	0.0009375	5.77(1)	737(35)	17(1)

TABLE II: A list of the pseudo-critical gauge coupling $\beta_c(m_q)$ and the peak height of the disconnected chiral susceptibility $\chi^c_{q,disc}/T^2$ as well as the chiral condensate at the pseudo-critical gauge coupling $\langle\bar\psi\psi\rangle^c_q/T^3$ for various quark masses and volumes.

scalings are found to hold for a window of quark masses then one can estimate bounds on the critical value for the pseudo-scalar Goldstone mass. As we do not know the value of the critical quark mass in 3-flavor QCD, it is at present not possible to determine the proper order parameter, e.g. from linear combinations of the chiral condensate and the gauge action, $M = \bar\psi\psi + sS_G$ [10]. At present we thus cannot perform a scaling analysis based on the construction of the magnetic equation of state, c.f. Eq. (5). Instead, we will try to make use of the scaling behavior of the disconnected part of the chiral susceptibility at the pseudo-critical gauge coupling (temperature), i.e. we will use Eq. (12) to estimate the critical pion mass.

First of all we need to determine the values of chiral observables at the pseudo-critical values, $\beta_c(m_q)$, of the gauge coupling where the disconnected susceptibility peaks. We performed cubic spline fits to $\chi_{q,disc}/T^2$. Since we generally have about 8 data points (β values) at each quark mass we mostly use three knots in the spline fit to keep a larger number of degrees of freedom, i.e. larger or equal to 3. Two of the knots are fixed at the boundary of the β-range and the third knot is varied within the β-range. The fit results for chiral condensates and susceptibilities we have shown in the figures of this paper, e.g. in Fig. 1, have been obtained by choosing the third knot such that the resulting $\chi^2/d.o.f$ is closest to unity. To determine the pseudo-critical couplings, β_c, we performed cubic spline fits for the disconnected part of the chiral susceptibilities using the bootstrap method, where fits with $\chi^2/d.o.f$ closest to unity are chosen. The value and error of the disconnected part of the chiral susceptibility at β_c is obtained in the same way. The value β_c for different quark masses and lattice sizes, the peak height of the disconnected part of the chiral susceptibility $\chi_{q,disc}/T^2$ and the value of the chiral condensate at β_c, $\langle\bar\psi\psi\rangle^c_q/T^3$, are listed in Table II. We also estimated systematic uncertainties of our fits by performing cubic spline fits of the disconnected part of the chiral susceptibility with the third knot chosen such that the $\chi^2/d.o.f$ is farthest away from unity. This results in values for β_c and $\chi^c_{\rm q,disc}/T^2$ that are within the uncertainties of those listed in Table II. Note that the current way of performing spline fits also brings in some artifacts, e.g. the unphysical dips seen in the right plots of Fig. 1 and Fig. 3 near the smallest β-values. These dips can be cured by relocating the knots. However, the resulting changes of $\beta_c(m_q)$, $\langle\bar\psi\psi\rangle^c_q$ and $\chi^c_{q,disc}$ are small and well included within the uncertainties mentioned before.

Since in 3-flavor QCD the scaling variables are mixtures of $\Delta\beta$ and Δm (c.f. Eq. (9)) also the scaling behavior of the order parameter in the quark mass becomes complicated due to this mixture. In the immediate vicinity of the critical point, the t-direction i.e. the line $h = 0$ is defined as the tangent to the pseudo-critical line [10]. In the limit $\Delta\beta \to 0$ the mixing coefficient B can then be determined from

$$\frac{d\beta_c(m_q)}{dm_q} = -1/B. \qquad (15)$$

The dependence of the pseudo-critical coupling, $\beta_c(m_q)$, on the quark mass is shown in Fig. 6. Shown also in Fig. 6 are two fits using as ansatz the leading linear term in Eq. (11) in two different fitting ranges. These fits obviously yield an upper bound on the absolute value of the mixing parameter B. From these fits we find that B is in the range of $-0.038 \lesssim B \le 0$. Thus the scaling behavior of the chiral observables will be described by corresponding relations in Eqs. (12) and (13). However, the mixing is small. This has consequences for the scaling of e.g. the peak in the chiral susceptibility. Although for any $B < 0$ the peak height will diverge with the critical exponent γ, this behavior sets in only for very small values of the quark mass. In general one will see an effective exponent γ_{eff}, which will closely resemble the situation at $B = 0$, i.e. $\gamma_{eff} \simeq 1 - 1/\delta$. This can be seen from the fits to the peak heights of

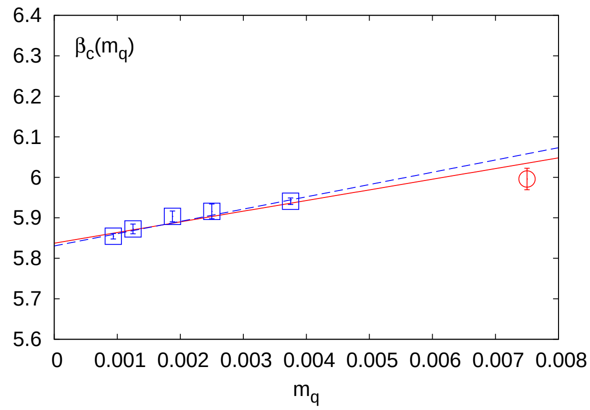

FIG. 6: β_c as a function of quark mass m_q. The red solid and blue dashed lines represent linear fits using an ansatz of $-m_q/B+c$ with and without the data point at the heaviest quark mass, respectively.

disconnected chiral susceptibilities with an ansatz of $b(m_q-m_q^c)^{\gamma_{eff}}$ where γ_{eff} is a fit parameter. The fit results are shown in the left plot of Fig. 7. The fit to the entire quark mass region is denoted by the purple solid line and it gives $\chi^2/d.o.f=0.88$ and (m_q^c,γ_{eff})=(0.0004(1), 0.78(6)). We also investigate the dependence of fit results on the fit range. A fit leaving out the largest quark mass (denoted by the red solid line) yields $\chi^2/d.o.f=0.44$ and (m_q^c,γ_{eff})=(0.00012(19)), 0.95(11)) while the fit leaving out the two largest quark masses (denoted by the blue solid line) gives $\chi^2/d.o.f=0.004$ and (m_q^c,γ_{eff})=(0.0004(2), 0.70(1)).

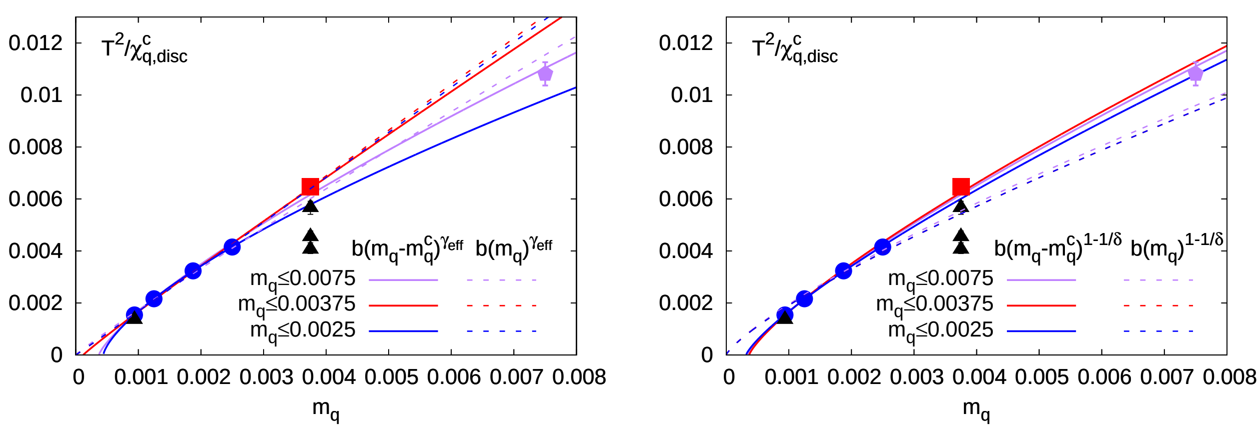

FIG. 7: The inverse of the maxima of the disconnected chiral susceptibility versus the bare quark mass, m_q. The solid lines and dashed lines show fits based on a scaling ansatz $b(m_q-m_q^c)^{exponent}$ and $b(m_q)^{exponent}$, respectively. The fit results shown in the left plot were obtained using an exponent of γ_{eff} as a free parameter while in the right plot the exponent being fixed to $1-1/\delta$. The fits with different upper limits for the fit range in the quark mass, i.e. 0.0075, 0.00375 and 0.0025 are also shown. The black triangles represent the data points for smaller volumes, i.e. N_s=16 with $m_q=0.0009375$ and $N_s=16$, 12 and 10 with $m_q=0.00375$. For more details see discussions given in the text.

We thus have fixed γ_{eff} to $1-1/\delta$ in the following analysis. In the right plot of Fig. 7 we show the fit results for $T^2/\chi_{q,disc}$ by using the ansatz $b\,(m_q-m_q^c)^{1-1/\delta}$. The critical quark mass m_q^c can easily be obtained from the intercept of the fitting function and the quark mass axis. The fit to the whole quark mass region has a $\chi^2/d.o.f.$=0.67. It is shown in the right plot of Fig. 7 labeled by the purple solid line. The estimated critical quark mass is $m_q^c=0.00035(3)$ with only the uncertainty from the fit. This corresponds to $m_\pi^c\simeq 50$ MeV. We also consider uncertainties arising from the fit range, i.e. the validity range of the scaling ansatz used for our fit. We did this by fitting to data without the data point at the largest quark mass, i.e. $m_q=0.0075$. The $\chi^2/d.o.f.$ which resulted from the fit (denoted as the red solid line) without the data point at $m_q = 0.0075$ remains almost the same. It gives a similar critical quark mass value $m_q^c = 0.00037(4)$. While omitting the third heaviest quark mass in the fit results in a very small $\chi^2/d.o.f.$ i.e. 0.07. Nevertheless the obtained $m_q^c = 0.00032(2)$ is consistent with previous two estimates within errors. We also tried to fit the data with an ansatz motivated by the scaling behavior in the 3-dimensional Z(2) universality class but with a vanishing critical quark mass m_q^c. The ansatz thus is $T^2/\chi^c_{q,disc} = b\ m_q^{1-1/\delta}$ with only one fit parameter b. Such a fit obviously cannot describe the data at all [4], as can be seen from dashed lines in the right plot of Fig. 7. However, an ansatz of $bm_q^{\gamma_{eff}}$ can describe the data well when the largest two quark masses are excluded from the fit as shown in the left plot of Fig. 7. We thus cannot rule out that m_q^c can actually be zero.

In Fig. 7 we also show $T^2/\chi^c_{q,disc}$ obtained for different volumes at the second highest and the smallest quark masses as the black triangles. Since $T^2/\chi^c_{q,disc}$ reduces with decreasing volume, it is expected that effects arising from a finite volume overestimate m_q^c, i.e. in the thermodynamic limit m_q^c becomes smaller. Note that in our current simulations with $N_s = 24$ even for the lightest quark mass the finite volume effects are expected to be less than 10% on $T^2/\chi^c_{q,disc}$ and consequently the change in the estimate of m_q^c in the thermodynamic limit is moderate. With the limitations of finite volume effects and the fit results shown in Fig. 7, at present, we can only provide an estimate for the upper bound of the critical pion mass, $m_\pi \simeq 50$ MeV [5]. This result is compatible with that obtained from calculations using the stout action on $N_t = 6$ lattices [19].

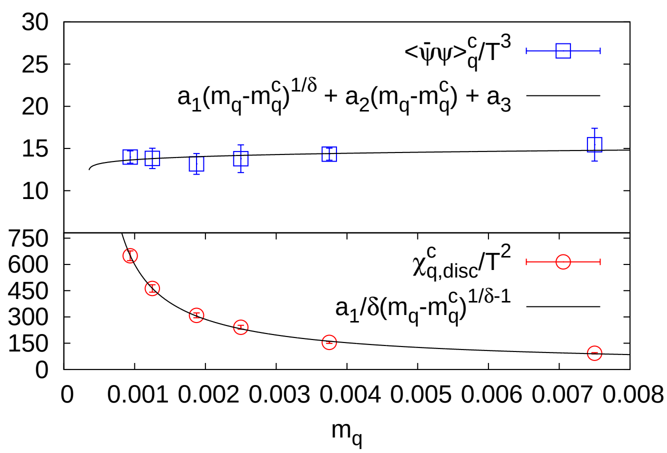

FIG. 8: A simultaneous joint fit using a 4-parameter ansatz to both light quark chiral condensate and the disconnected part of its susceptibility at β_c.

To have a better understanding of the uncertainties in the estimate of m_q^c we also take into account possible contributions arising from the regular part of chiral observables, i.e. for the chiral condensate we use a fit ansatz of the form $a_1(m_q - m_q^c)^{1/\delta} + a_2(m_q - m_q^c) + a_3$. Here, a_2 includes contributions from an m_q-type additive ultraviolet divergent term, as well as the regular part of the chiral susceptibility, and a non-vanishing a_3 reflects that the chiral order parameter is not the correct order parameter and will approach a non-vanishing value at (m_q^c, β_c) . Since this involves four fit parameters and we only have six data points corresponding to the six different quark masses, we performed a joint fit to both the chiral condensate and the disconnected part of the chiral susceptibility. For the fit to the disconnected part of the chiral susceptibility we assume that the singular behavior of chiral condensate is completely encoded within the disconnected chiral susceptibility, and not partly within the connected part of the chiral susceptibility. Further, the disconnected chiral susceptibility does not contain $1/a^2$ power-law divergences, and we assume that any additional contribution from the regular part of the chiral condensate to a diverging chiral susceptibility can be neglected. Thus, for the disconnected chiral susceptibility we use as a fit ansatz $a_1/\delta \cdot (m_q - m_q^c)^{1/\delta-1}$. Results from such a combined fit are shown in Fig. 8. This yields $a_1 = 8.6(2)$, $m_q^c = 0.00035(3)$ and

[4] In the case m_q^c=0 one would, of course, expect that $O(N)$ critical exponents are more relevant than the Z(2). These critical exponents, however, are quite similar and would not change the conclusion given here.

[5] We will nevertheless show in Appendix B the fit results with a critical exponent of γ which supports current upper bound of m_q^c.

a_3=11.8(4) with $\chi^2/d.o.f = 0.46$. The value of a_1 is consistent with δ/b where $b = 0.55(1)$ is obtained from the fit shown in the right plot of Fig. 7. The current estimate of m_q^c is within the upper bound we obtained before, and the nonzero value of a_3 is certainly consistent with a nonzero value of m_q^c. The consistency can be understood since the chiral condensate is not a true order parameter as discussed in the Appendix A. This estimate on m_q^c is consistent with what we obtained from the fit shown in Fig. 7. We also performed similar joint fits by taking into account a regular contribution to the disconnected chiral susceptibility with an ansatz $a_1/\delta(m_q - m_q^c)^{1/\delta-1} + a_4$. Within errors, the fitted values of a_1 and m_c were found to be consistent with the previous case while a_4 turned out to be vanishingly small compared to a_2.

V. CONCLUSION

We carried out calculations for 3-flavor QCD using the HISQ action on $N_t = 6$ lattices. We used six values of pion masses in the mass range 80 MeV $\lesssim m_\pi \lesssim$ 230 MeV. From the study of chiral condensates and chiral susceptibilities we found no direct evidence for the existence of a first order chiral phase transition in this pion mass region. Assuming that the quark masses used in this study lie within the critical scaling window of the anticipated chiral critical point of the 3-flavor QCD, we investigated 3-d Z(2) scaling behaviors of the chiral observables. Relying on these scaling studies, we were able to estimate an upper bound of the critical pion mass, i.e. $m_\pi \lesssim 50$ MeV. As pointed out before, estimates of critical pion masses tend to yield smaller values as one approaches closer to the continuum limit, either by going to finer lattice spacings or through using improved actions. While, in future, it will be essential to carry out lattice QCD calculations for smaller quark masses and closer to the continuum limit to establish the first order chiral phase transition region of 3-flavor QCD, and it is likely that this region will remain bounded by the critical pion mass estimated in the present study. The estimated smallness of the critical pion mass for 3-flavor QCD suggests that the first order chiral phase transition region of 3-flavor QCD might have little influence on the phase structure of physical QCD, both for zero and non-zero baryon chemical potential.

Acknowledgments

The numerical simulations were carried out on clusters of the USQCD Collaboration in Jefferson Lab and Fermilab, and on BlueGene/L computers at the New York Center for Computational Sciences (NYCCS) at Brookhaven National Lab, and on the local computing cluster at Central China Normal University. The work is partly supported by the U.S. Department of Energy under Contract No. DE-SC0012704, the Bundesministerium für Bildung und Forschung (BMBF) under grant no. 05P15PBCAA, National Natural Science Foundation of China under grant numbers 11535012 and 11521064, and the Early Career Research Award of the Science and Engineering Research Board of the Government of India.

Appendix A: General behavior of order parameter and chiral condensate

We want to discuss here the scaling behavior of the chiral condensate and its susceptibility at a possible critical point in the coupling - quark mass plane which belongs to the 3-dimensional Z(2) universality class. At this critical point the chiral condensate itself is not a true order parameter, but is part of a mixture of operators that define the true order parameter M.

The behavior of the order parameter M for this phase transition as a function of the quark mass at different values of temperature is depicted in the left plot of Fig. 9. At fixed temperature the order parameter M decreases when decreasing the external field h. From Eq. (9) it follows that this corresponds to a decreasing quark mass,

$$m_q = h_0 h + m_q^c - B(\beta - \beta_c) \ . \tag{16}$$

The $h = 0$ line is indicated in Fig. 9 by a dashed (red) line. For $B < 0$ the lines of constant temperature, i.e. constant β, will end for $h = 0$ at coordinates of $(M > 0, m_q < m_q^c)$ in the $M - m_q$ plane in the symmetry broken phase where $\beta < \beta_c$ and at $(M = 0, m_q \geq m_q^c)$ in the symmetry restored phase where $\beta > \beta_c$. In particular at $T = T_c(m_q = m_q^c)$ and $m_q = m_q^c$ the line of constant temperature ends at $M = 0$ marked by a big blue dot in the left plot of Fig. 9. When changing the external field h from positive to negative values at $T < T_c(m_q = m_q^c)$ the order parameter M will change discontinuously, i.e. this temperature range corresponds to the first order transition region in 3-flavor QCD. Finally at temperatures lower than the critical temperature in the chiral limit, i.e. when $T < T_c(m_q = 0)$ no phase transition occurs, irrespective of the value of quark mass. For any value of the quark mass the system is in the spontaneously broken phase.

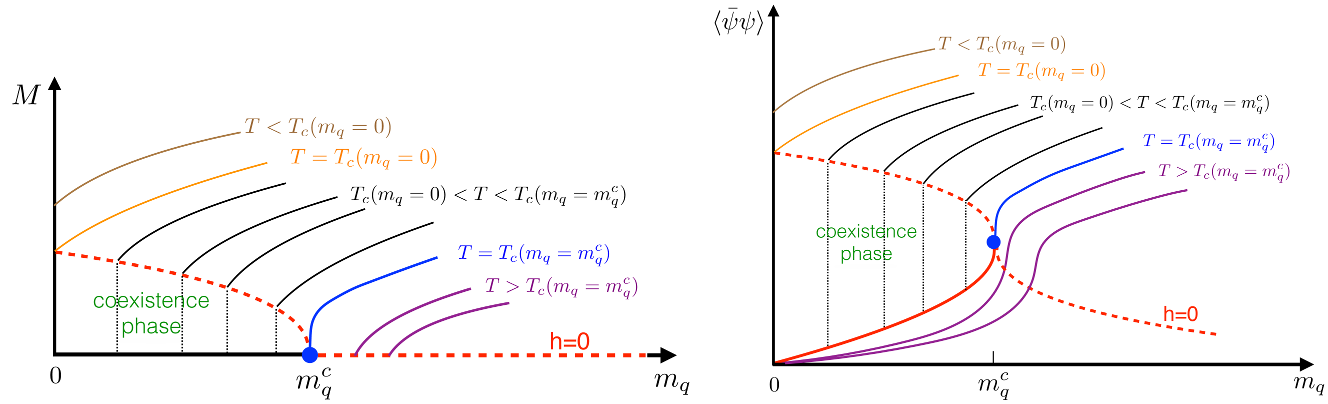

FIG. 9: Left: The order parameter M of the phase transition in the 3-flavor QCD as a function of quark masses at different temperatures. Right: Same as the left plot but for the chiral condensate. Here $T_c(m_q)$ is the (pseudo-) critical temperature of QCD with different values of quark masses m_q. The red dashed line indicates the line of vanishing external field, $h = 0$, and the blue dots mark the location of the critical point at $T = T_c(m_q^c)$.

The situation is similar for the quark chiral condensate $\langle\bar{\psi}\psi\rangle$, which obviously is not the order parameter for 3-flavor QCD. However, for small values of the mixing parameter B, it is a dominant component of the order parameter. We sketch its behavior in Fig. 9 (right). Of course, the relation between m and h given by Eq. (16) remains the same in this case. However, the y-coordinate for the line corresponding to $h = 0$ gets distorted because $\langle\bar{\psi}\psi\rangle$ stays finite at the critical point (β_c, m_c), which is marked also by a big blue dot in the right hand part of Fig. 9. From this it is apparent that also for $T > T_c(m_q = m_q^c)$ and $m_q > m_q^c$ the chiral condensate $\langle\bar{\psi}\psi\rangle$ does not vanish at $h = 0$ as it is not the proper order parameter. The h=0 line is also indicated by a dashed line in the figure. Also note that at the temperature corresponding to the chiral limit ($T = T_c(m_q = 0)$) the chiral condensate drops from a finite value directly to zero.

In general we have no direct access to the order parameter itself, which needs to be constructed from e.g. a linear combination of the chiral condensate and the gauge action. For our purpose, however, it is sufficient to relate the chiral condensate and its susceptibility to the singular part of the free energy introduced in Eqs. (3) and (4). For the contribution of the singular part of the free energy to the chiral condensate we then obtain

$$\langle\bar{\psi}\psi\rangle_{sing} = h^{1/\delta}\tilde{f}_G(t,h) \ , \tag{17}$$

with t and h introduced in Eqs. (8) and (9), respectively. For $A = B = 0$ the function $\tilde{f}_G(t,h)$ reduces to the scaling function $f_G(z)$. However for $A \neq 0$, t as well as h depend on the quark mass and $\tilde{f}_G$ thus receives contributions from partial derivatives of both arguments of f_{sing}

$$\begin{aligned}
\tilde{f}_G(t,h) &= -\Big(1+\frac{1}{\delta}\Big)f_s(z) - \frac{1}{\beta\delta}\frac{\partial z}{\partial m_q}\frac{\partial f_s(z)}{\partial z} \\
&= -\Big(1+\frac{1}{\delta}\Big)f_s(z) - \frac{z}{\beta\delta}\Big(A\beta\delta\frac{h}{t}-1\Big)\frac{\partial f_s(z)}{\partial z} \\
&= f_G(z) - Ah^{\omega}\frac{\partial f_s(z)}{\partial z}\frac{h_0}{t_0} \quad ,
\end{aligned} \tag{18}$$

with $\omega = 1 - 1/\beta\delta$. In general, the singular part of the free energy thus does not lead to a simple scaling form of the chiral condensate. It receives corrections to scaling, which relative to the h-dependence of the chiral condensate, are suppressed by a factor $h^{\omega} \simeq h^{1/2}$.

Similarly we can analyze the scaling properties of the chiral susceptibility,

$$\chi_q = \frac{\partial\langle\bar{\psi}\psi\rangle}{\partial m_q} \ . \tag{19}$$

The singular contribution to χ_q can then be obtained from Eq. (18),

$$\chi_q^{sing} = \frac{\partial\langle\bar{\psi}\psi\rangle_{sing}}{\partial m_q} = \frac{1}{h_0}h^{1/\delta-1}\tilde{f}_\chi(t,h) \ , \tag{20}$$

with

$$\tilde{f}_\chi(t,h) = f_\chi(z) + Ah^\omega \frac{h_0}{t_0} P_1(z) + \left(Ah^\omega \frac{h_0}{t_0} \right)^2 P_2(z) \; , \tag{21}$$

and

$$\begin{aligned} P_1(z) &= f'_G(z) - (\omega + \frac{1}{\delta}) f'_s(z) + \frac{z}{\beta\delta} f''_s(z) \; , \\ P_2(z) &= -f''_s(z) \; . \end{aligned} \tag{22}$$

One thus finds that the chiral susceptibility diverges in the vicinity of the critical point just like the order parameter susceptibility, i.e. $\chi_q \sim h^{1/\delta - 1}$, as shown in Eq. (12).

In order to make sure that the scaling arguments given in connection with Eq. (12) are valid also for a pseudo-critical coupling extracted from the location of a peak in the chiral susceptibility rather than the true order parameter M, we also need to check that the locaton of this peak corresponds to a constant value of the scaling variable z. I.e. in the chiral limit the peak is located at some position $z = z_c$. Ignoring the corrections to scaling in Eq. (20) we may determine the location of the peak of χ_q at fixed quark mass. We need to solve

$$\begin{aligned} 0 &= \frac{\partial}{\partial\beta} h^{1/\delta - 1} f_\chi(z) \\ &= B \left(\frac{1}{\delta} - 1 \right) f_\chi(z) - \left(h^\omega - \frac{B}{\beta\delta} z \right) f'_\chi(z) \; , \end{aligned} \tag{23}$$

Obviously for $B = 0$ the peak of χ_q at fixed quark mass corresponds to the peak of $f_\chi(z)$, i.e. z_p. For $B \neq 0$ Eq. (23) is a function of the scaling variable z aside from some corrections to scaling that are proportional to h^ω. The location of the peak in the chiral susceptibility thus is controlled by a value of the scaling variable $z = z_c$ up to some corrections to scaling that vanish in the limit $h \to 0$. For small values of B we can determine z_c by expanding around $z = z_p$, i.e. $\Delta z/z_p = z_c/z_p - 1 = B(1/\delta - 1) f_\chi(z_p) \Big/ \left(z_p^2 f''_\chi(z_p) (\frac{h}{t}|_{z_p} \frac{h_0}{t_0} - \frac{B}{\beta\delta}) \right)$.

Appendix B: Mixing coefficient and effective critical exponent

As seen from Eq. (11), the dominant term determining the relation between $\Delta\beta$ and Δm in the limit $\Delta\beta \to 0$ is proportional to B, which will be small in QCD when the critical quark mass is small. Outside a small asymptotic scaling region the second term in Eq. (11) thus will be dominant and χ_M may show an effective scaling controlled by the exponent $1 - 1/\delta$. To illustrate this we consider the simple scaling form

$$\chi_M^{peak} \sim h^{1/\delta - 1} \sim \left((1+B^2)\Delta\beta - B \left(z_0/z_p \, (1+B^2)\Delta\beta \right)^{\beta\delta} \right)^{-\gamma} \; , \tag{24}$$

where we used Eqs. (10) and (11) to express the external field h, introduced in Eq. (9), in terms of $\Delta\beta$ only.

We show in Fig. 10 the effective exponent γ_{eff} describing the behavior of χ_M^{peak} as function of $\Delta\beta$. This shows that we may expect to find a rather complicated scaling behavior of χ_M^{peak}. We can see that as long as the value of B is small the effective exponent is much closer to $1 - 1/\delta$ rather than γ in most cases that might apply to our current investigation .

As discussed above and also in Section IV C the effective critical exponent is expected to be rather close to $1/\delta - 1$. We nevertheless would like to check the uncertainties in the estimate of the critical quark mass arising from the critical exponents. We thus use an ansatz of $b(m_q - m_q^c)^\gamma$ to fit the inverse of the disconnected part of the chiral susceptibilities at $\beta_c(m_q)$. The fit result is shown in Fig. 11. All the fits to the data sets with all the masses, without the heaviest mass point and without two heaviest mass points prefer negative values of m_q^c which can be seen clearly from the intercept of the solid lines with the x axis.

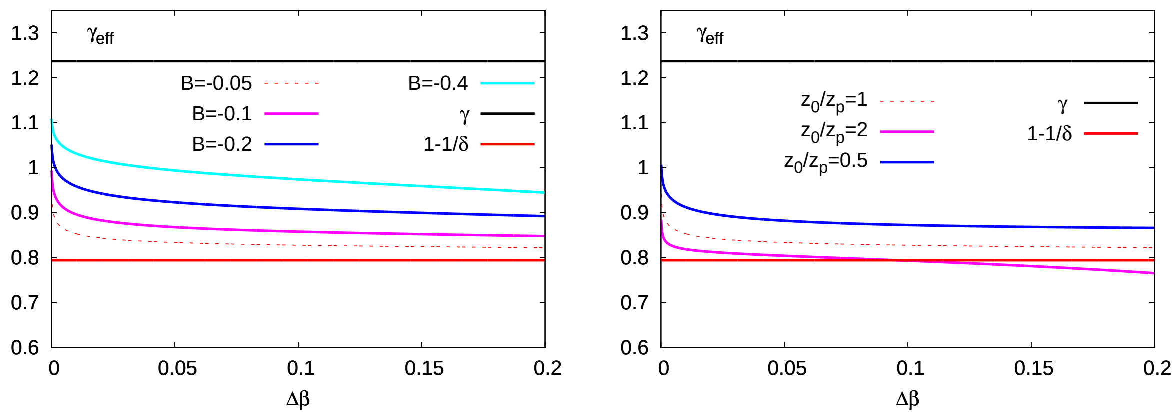

FIG. 10: The effective scaling exponent, $\gamma_{eff} = -\ln(\chi_M^{peak})/\ln(\Delta m)$, extracted from the peak value of the order parameter susceptibility obtained from Eq. (24). Here $\gamma_{eff} = \gamma$ when B=0. Left: For $z_0/z_p = 1$ and several values of the mixing coefficient B. Right: For $B = -0.05$ and several different values of z_0/z_p.

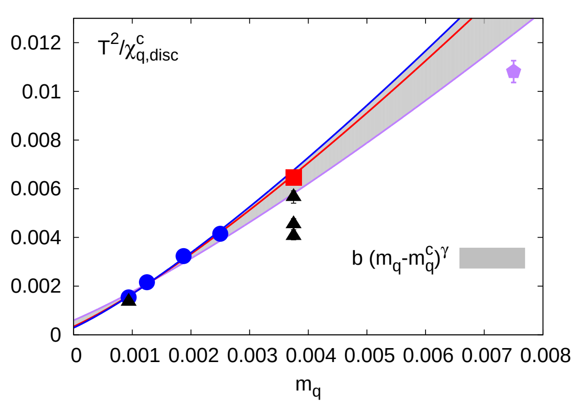

FIG. 11: Fits to $T^2/\chi^c_{q,disc}$ using an ansatz of $b(m_q - m_q^c)^\gamma$. The purple, red and blue line represents the fit to the whole quark mass region, $m_q < 0.0075$ and $m_q < 0.00375$, respectively.

[1] R. D. Pisarski and F. Wilczek, *Remarks on the Chiral Phase Transition in Chromodynamics*, *Phys.Rev.* **D29** (1984) 338–341.

[2] C. Schmidt, C. Allton, S. Ejiri, S. Hands, O. Kaczmarek et al., *The Quark mass and mu dependence of the QCD chiral critical point*, *Nucl.Phys.Proc.Suppl.* **119** (2003) 517–519, [hep-lat/0209009].

[3] P. de Forcrand and O. Philipsen, *The Chiral critical point of N(f) = 3 QCD at finite density to the order (mu/T)**4*, *JHEP* **11** (2008) 012, [0808.1096].

[4] X.-Y. Jin, Y. Kuramashi, Y. Nakamura, S. Takeda and A. Ukawa, *Curvature of the critical line on the plane of quark chemical potential and pseudoscalar meson mass for three-flavor QCD*, *Phys. Rev.* **D92** (2015) 114511, [1504.00113].

[5] S. Gupta, *Phases and properties of quark matter*, *J. Phys.* **G35** (2008) 104018, [0806.2255].

[6] N. Christ and X. Liao, *Locating the 3-flavor critical point using staggered fermions*, *Nucl.Phys.Proc.Suppl.* **119** (2003) 514–516.

[7] P. de Forcrand and O. Philipsen, *The Phase diagram of N(f) = 3 QCD for small baryon densities*, *Nucl.Phys.Proc.Suppl.* **129** (2004) 521–523, [hep-lat/0309109].

[8] P. de Forcrand, S. Kim and O. Philipsen, *A QCD chiral critical point at small chemical potential: Is it there or not?*, *PoS* **LAT2007** (2007) 178, [0711.0262].

[9] D. Smith and C. Schmidt, *On the universal critical behavior in 3-flavor QCD*, *PoS* **LATTICE2011** (2011) 216, [1109.6729].

[10] F. Karsch, E. Laermann and C. Schmidt, *The Chiral critical point in three-flavor QCD*, *Phys.Lett.* **B520** (2001) 41–49, [hep-lat/0107020].

[11] F. Karsch, C. Allton, S. Ejiri, S. Hands, O. Kaczmarek et al., *Where is the chiral critical point in three flavor QCD?*, *Nucl.Phys.Proc.Suppl.* **129** (2004) 614–616, [hep-lat/0309116].

[12] MILC collaboration, C. Bernard et al., *QCD thermodynamics with three flavors of improved staggered quarks*, *Phys.Rev.* **D71** (2005) 034504, [hep-lat/0405029].

[13] M. Cheng, N. Christ, M. Clark, J. van der Heide, C. Jung et al., *Study of the finite temperature transition in 3-flavor QCD using the R and RHMC algorithms*, *Phys.Rev.* **D75** (2007) 034506, [hep-lat/0612001].

[14] X.-Y. Jin, Y. Kuramashi, Y. Nakamura, S. Takeda and A. Ukawa, *Critical endpoint of the finite temperature phase transition for three flavor QCD*, *Phys.Rev.* **D91** (2015) 014508, [1411.7461].

[15] S. Takeda, X.-Y. Jin, Y. Kuramashi, Y. Nakamura and A. Ukawa, *Update on Nf=3 finite temperature QCD phase structure with Wilson-Clover fermion action*, in *Proceedings, 34th International Symposium on Lattice Field Theory (Lattice 2016): Southampton, UK, July 24-30, 2016*, 2016. [1612.05371].

[16] A. Hasenfratz and F. Knechtli, *Four flavor finite temperature phase transition with HYP action: Where is the first order endpoint?*, hep-lat/0105022.

[17] C. Bonati, P. de Forcrand, M. D'Elia, O. Philipsen and F. Sanfilippo, *Chiral phase transition in two-flavor QCD from an imaginary chemical potential*, *Phys.Rev.* **D90** (2014) 074030, [1408.5086].

[18] O. Philipsen and C. Pinke, *The $N_f = 2$ QCD chiral phase transition with Wilson fermions at zero and imaginary chemical potential*, *Phys. Rev.* **D93** (2016) 114507, [1602.06129].

[19] G. Endrodi, Z. Fodor, S. Katz and K. Szabo, *The Nature of the finite temperature QCD transition as a function of the quark masses*, *PoS* **LAT2007** (2007) 182, [0710.0998].

[20] H.-T. Ding and P. Hegde [Bielefeld-BNL-CCNU collaboration], *Chiral phase transition of N_f=2+1 and 3 QCD at vanishing baryon chemical potential*, *PoS* **LATTICE2015** (2016) 161, [1511.00553].

[21] H.-T. Ding, A. Bazavov, P. Hegde, F. Karsch, S. Mukherjee et al., *Exploring phase diagram of $N_f = 3$ QCD at $\mu = 0$ with HISQ fermions*, *PoS* **LATTICE2011** (2011) 191, [1111.0185].

[22] H.-T. Ding, *Exploring QCD phase diagram at vanishing baryon density on the lattice*, *J.Phys.Conf.Ser.* **432** (2013) 012027, [1302.5740].

[23] HPQCD, UKQCD collaboration, E. Follana et al., *Highly improved staggered quarks on the lattice, with applications to charm physics*, *Phys.Rev.* **D75** (2007) 054502, [hep-lat/0610092].

[24] H.-T. Ding, F. Karsch and S. Mukherjee, *Thermodynamics of strong-interaction matter from Lattice QCD*, *Int. J. Mod. Phys.* **E24** (2015) 1530007, [1504.05274].

[25] A. Bazavov, T. Bhattacharya, M. Cheng, C. DeTar, H. Ding et al., *The chiral and deconfinement aspects of the QCD transition*, *Phys.Rev.* **D85** (2012) 054503, [1111.1710].

[26] HotQCD collaboration, A. Bazavov et al., *Equation of state in (2+1)-flavor QCD*, *Phys.Rev.* **D90** (2014) 094503, [1407.6387].

[27] S. El-Showk, M. F. Paulos, D. Poland, S. Rychkov, D. Simmons-Duffin and A. Vichi, *Solving the 3d Ising Model with the Conformal Bootstrap II. c-Minimization and Precise Critical Exponents*, *J. Stat. Phys.* **157** (2014) 869, [1403.4545].

[28] S. Ejiri, F. Karsch, E. Laermann, C. Miao, S. Mukherjee et al., *On the magnetic equation of state in (2+1)-flavor QCD*, *Phys.Rev.* **D80** (2009) 094505, [0909.5122].

[29] F. Karsch, *O(N) universality and the chiral phase transition in QCD*, *Prog.Theor.Phys.Suppl.* **186** (2010) 479–484, [1007.2393].

[30] S. Gavin, A. Gocksch and R. D. Pisarski, *QCD and the chiral critical point*, *Phys. Rev.* **D49** (1994) 3079–3082, [hep-ph/9311350].

[31] F. Karsch and S. Stickan, *The Three-dimensional, three state Potts model in an external field*,

Phys. Lett. **B488** (2000) 319–325, [hep-lat/0007019].

[32] J. Engels and F. Karsch, *Finite size dependence of scaling functions of the three-dimensional O(4) model in an external field*, *Phys. Rev.* **D90** (2014) 014501, [1402.5302].

[33] J. Engels, S. Holtmann, T. Mendes and T. Schulze, *Finite size scaling functions for 3-d O(4) and O(2) spin models and QCD*, *Phys.Lett.* **B514** (2001) 299–308, [hep-lat/0105028].